

# **Channel Optimization Design - A Case Study of Shawan River, Shenzhen**

Teammates: Pan Xinxin (Leader), Wang Yalin, Zhao Lingzhen, Tang Jiatong

## ***Abstract:***

This study investigates the optimization of the Shawan River channel in Shenzhen to enhance flood protection and balance sedimentation prevention with erosion control. Using MIKE and FLOW-3D models, the performance of natural and optimized channels under different flow conditions, including a 100-year return period storm, is analyzed. Results show that the optimized channel improves stability and efficiency, particularly in extreme conditions. A comparison of trapezoidal weirs with varying slopes highlights that milder slopes increase flow capacity, while steeper slopes heighten shear stress and erosion risks. These findings offer valuable insights for effective channel design.

## ***Keywords:***

Stable Flow; TKE; Sediment Transport; Weir Shape.

## 1. Introduction

For flood protection in open channel design within fluvial processes, several critical principles must be followed to achieve the dual objectives of enhancing flood protection and conserving ecosystems [1]:

- 1) Increase the average channel width;
- 2) Decrease the average flow depth and velocity to balance sedimentation prevention with erosion control;
- 3) Installing submerged trapezoidal weirs to manage sediment transport, regulate flow velocity, and control discharge.

To verify the effectiveness of channel optimization design and the associated hydraulic characteristics, a 900m-long Shawan river (Chainage: S3+570.21 ~ S4+470.05) (See Fig. 1) was selected as a case study. The Shawan River is part of the Pearl River Delta Basin, a crucial watershed in Shenzhen.

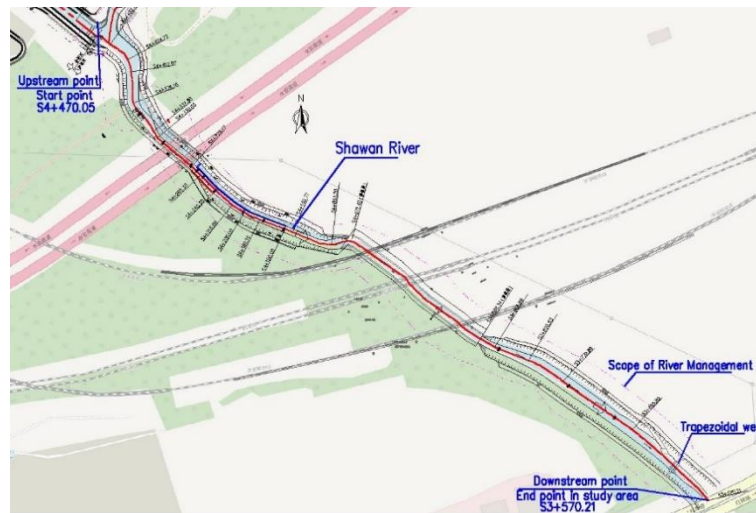


Fig. 1. 900-meter-long upstream in Shawan channel

The Shawan River optimization project in 2016 implemented several measures based on the above principles: [2]

- 1) Expanding the channel's bottom width;
- 2) Reshaping the channel cross-section into a trapezoidal form;
- 3) Installing submerged trapezoidal weirs to manage sedimentation and optimize flow velocity and discharge.

This study evaluates these principles with a focus on hydraulic properties, including:

- 1) Flow conditions in the natural versus optimized channels;
- 2) Determination of the appropriate upstream slope for weirs, considering the asymmetry of the weir cross-section.



Fig. 2. A long-term averaged flow state in weir

## 2. Methodology

### 2.1. Flow Computation in Optimized and Natural Channels

#### 2.1.1. Hydrological Model MIKE

DHI MIKE is one of the most widely used hydrodynamic models. It is used to simulate water surface profiles and discharge in rivers. [3] It solves the Saint-Venant equations, which describe the conservation of continuity and momentum, allowing for the simulation of fully dynamic wave behavior.

The MIKE HD module requires several data inputs, including a topographic map of the study area, river geometry, and time series data for water levels and discharge.

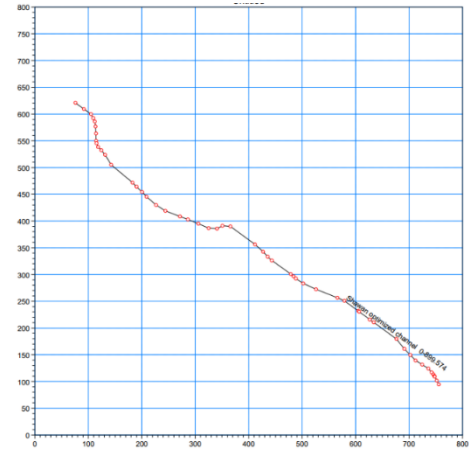


Fig. 3. River network in MIKE

The Q-h relationship is used as a boundary condition to model equilibrium flow.

#### 2.1.2. Flow Condition and Input Setup

Three flow conditions were modeled for analysis:

- 1) **Natural Channel:** Extreme discharge of  $Q=200m^3/s$  at the upstream boundary, representing a 100-year return period storm ( $P = 1\%$ ), with corresponding initial water levels at the downstream boundary.
- 2) **Optimized Channel:** Same boundary conditions (BCs) as scenario 1.
- 3) **Natural Channel:** Long-term averaged discharge of  $Q=50m^3/s$  at the upstream boundary ( $P=50\%$ ), with corresponding water level at the downstream boundary.

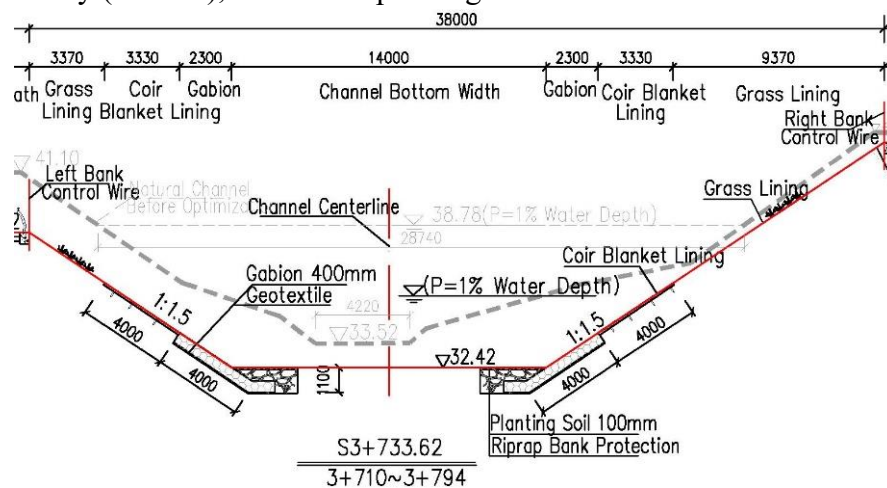


Fig. 4. Optimization channel section

The river geometry was defined by inputting cross-sections at approximately 50-meter intervals along the channel.

Considering the different Manning's coefficient  $n$ ,  $n=0.030$  for Natural channel with sand bed, and  $n=0.025$  for Optimized channel with Coir Blanket Lining (See Fig. 4).

### 2.1.3. Froude Number

The Froude number ( $Fr$ ) is generally calculated using the following equation:

$$Fr = \frac{V}{\sqrt{gh}} \quad (2-1)$$

Where:

- $V$  is the flow velocity,
- $g$  is the acceleration due to gravity, and
- $h$  is the flow depth.

The ideal minimum value of the Froude number ( $Fr_{min}$ ) can be determined through simulation. These simulations are based on several key assumptions:

- 1) The sand-bed river channel is alluvial.
- 2) Adjustments to the slope and cross-sectional shape of the channel must satisfy the equilibrium conditions for water and sediment transport.
- 3) These adjustments are related to the resistance provided by bed forms and sediment particles to the flow.

In this project, a minimum value of  $Fr$  can be calculated from the simulation results,, which corresponds to a particular set of hydraulic geometry parameters. For other variables, such as stream power per unit length (slope) and per unit weight of water, as well as flow resistance, no minimum values were found. However, the minimum Froude number ( $Fr_{min}$ ) represents a unique and stable equilibrium state of the highest stability[4]. According to the analysis, this minimum Froude number indicates the most stable equilibrium condition for the system.

From laboratory tests [4], the following regression equation for  $Fr_{min}$  was derived:

$$Fr_{min} = K \times (V \times J)^b \quad (2-2)$$

Where:

- $b$  is almost constant;
- $K$  differs according to the size of sediment;
- $J$  is the slope.

The values of  $b$  and  $K$  can be considered constant for a given sediment type, with  $K$  depending on the sand and gravel diameter  $d$ . From the laboratory tests, the relationship between  $K$  and  $d$  was obtained as follows (Fig. 5).[4]

$$K = 4.49 \times d^{-0.186} \quad (2-3)$$

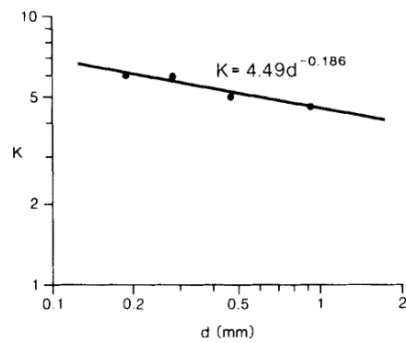


Fig. 5 The relation of  $K$  to  $d$

Thus, the final formula for  $Fr_{min}$  in this case is:

$$Fr_{min} = 4.49 \times d^{-0.186} \times (VJ)^b \quad (2-4)$$

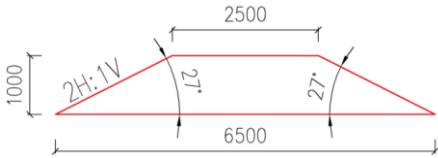
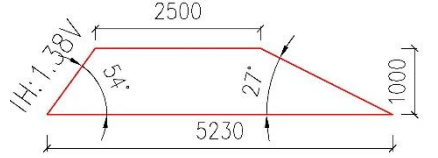
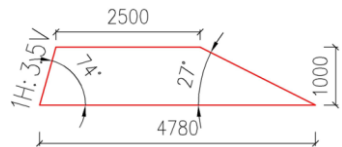
## 2.2. Configuration and Numerical Setup for Weirs

This study employs numerical simulations and corresponding case comparisons to analyze weir performance.

### 2.2.1. Flow and Weir Condition

To evaluate the impact of asymmetry in weir design on flow efficiency, three upstream weir slopes ( $\theta$ ) were selected based on reference tests[5]:  $27^\circ$ ,  $54^\circ$  and  $74^\circ$ . Additionally, the weir height ( $Z$ ) was set at 1 m, the weir crest length ( $L_{cr}$ ) at 2.5 m, and the downstream slope ( $\theta_d$ ) at  $27^\circ$ . These parameters represent an optimized design configuration (See Table. 1 for detailed weir design parameters and sketches).

Table. 1. Geometrical Conditions of Weirs

| Weir No. | Weir section   | Upstream slope $\theta$ | Upstream H:V | Weir Length(m) |
|----------|--|-------------------------|--------------|----------------|
| 1        |   | $27^\circ$              | 1:0.5        | 6.50           |
| 2        |   | $54^\circ$              | 1:1.38       | 5.23           |
| 3        |  | $74^\circ$              | 1:3.5        | 4.78           |

The simulated channel has a total length of 30 meters, with a fixed distance of 10 meters ( $L_I=10m$ ) between the upstream weir and the channel's starting point. A submerged flow condition was modeled with a water depth of  $H_0=1.5m$  to simulate a discharge of  $Q=50m^3/s$  ( $P=50\%$  corresponds to a long-term average water level). The initial water depth was set to 0.75 meters, which is 0.25 meters lower than the weir crest, to highlight the water-surface profile.

The downstream portion of the channel was modeled with a bottom width of 14 meters.

### 2.2.2. Numerical Setup

The FLOW-3D computational fluid dynamics (CFD) code was used for the simulations. This software utilizes the finite volume method to solve the Reynolds-averaged Navier-Stokes (N-S) equations and employs the Volume of Fluid (VOF) method to track free surface[6].

To optimize computational efficiency, a structured and mixed orthogonal mesh was used. Smaller cells (0.25 m) were applied in the weir region, while larger cells (0.5 m) were applied in the upstream and downstream sections (See Fig. 6~9). The total number of cells exceeded 60,000 for the 30-meter-long computational domain.

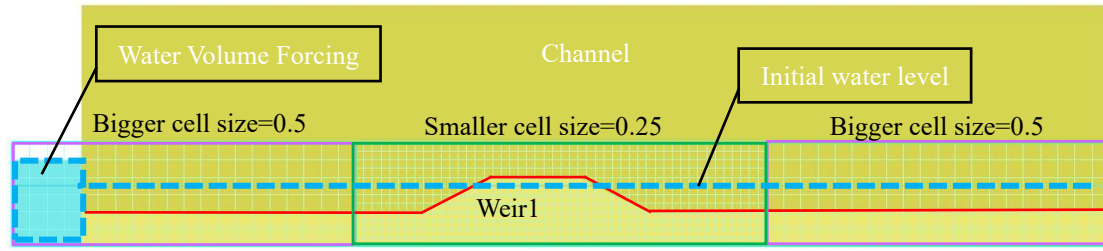


Fig. 6. Meshing in Y-Z Plane

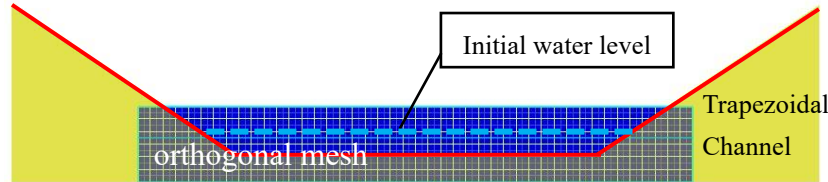


Fig. 7. Meshing in X-Z Plane

The Renormalization Group (RNG) turbulence model was employed to manage turbulent viscosity and prevent excessive values.

Flow data, including velocity and Froude number, were recorded at a specific location at the center of the weir along the Y-Z plane.

### 3. Analysis and Discussion

#### 3.1. Velocity Distribution of Channel Flow

This analysis focuses on velocity distribution at 14 selected locations within the channel. Using MIKE software, the Froude number for the natural (present) condition ( $Fr_{pre}$ ) and the optimized condition ( $Fr_o$ ) are obtained from the water depth and flow velocity data. The relevant data and flow profile are shown below.

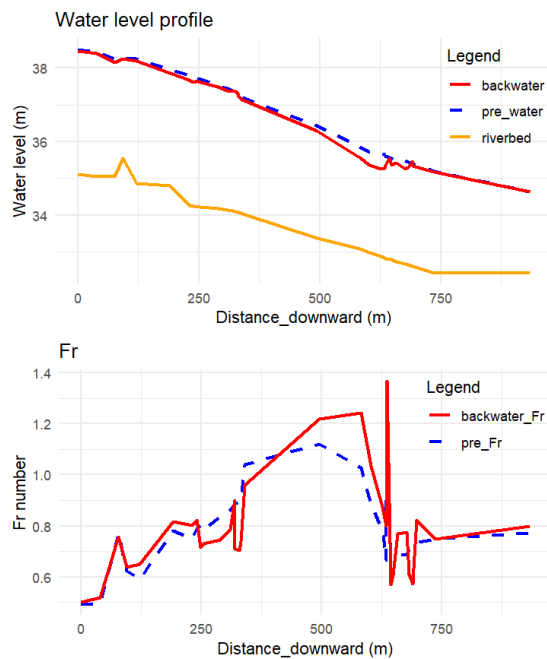


Fig. 8 Velocity and Fr profile

Table. 2. Calculation of Fr

| Distance | $Fr_{pre}$ | $Fr_o$ |
|----------|------------|--------|
| 0        | 0.39       | 0.64   |
| 76.45    | 0.41       | 0.93   |
| 93.95    | 0.53       | 0.54   |
| 122.05   | 0.63       | 0.78   |
| 191.05   | 1.27       | 0.9    |
| 230.05   | 1.14       | 1.15   |
| 320.05   | 0.95       | 1.33   |
| 406.45   | 1          | 0.83   |
| 453.04   | 1.37       | 0.99   |
| 494.72   | 1.17       | 1.01   |
| 581.71   | 1.14       | 1.33   |
| 633.73   | 0.87       | 0.88   |
| 736.43   | 0.77       | 0.96   |
| 844.05   | 0.83       | 1      |

Based on the available information for the Shawan River, the sand and gravel diameter  $d=0.2 \text{ mm}$ , which results in a  $b$ -value of about 0.377, as derived from JIA's work [4]. Use Equation(2-3), the K value was calculated as:

$$K = 4.49 \times 0.2^{-0.186} = 6.057.$$

From the design report, the average slope J of the channel is given as 0.002. Based on simulation results, the velocity V at the 14 locations in the natural state was calculated, yielding an average velocity  $V_{\text{mean}} = 1.86\text{m/s}$ .

Table. 3. Flow features form MIKE simulalating results

| Chainage      | Slope J | V     |
|---------------|---------|-------|
| 0             | 0.002   | 0.911 |
| 76.45         | 0.002   | 0.993 |
| 93.95         | 0.002   | 1.03  |
| 122.05        | 0.002   | 0.946 |
| 191.05        | 0.002   | 2.573 |
| 230.05        | 0.002   | 1.64  |
| 320.05        | 0.002   | 2.525 |
| 406.45        | 0.002   | 1.933 |
| 453.04        | 0.002   | 2.255 |
| 494.72        | 0.002   | 2.105 |
| 581.71        | 0.002   | 2.435 |
| 633.73        | 0.002   | 2.33  |
| 736.43        | 0.002   | 2.043 |
| 844.05        | 0.002   | 2.304 |
| Mean velocity |         | 1.86  |

Therefore, the ideal minimum Froude number of Shawan River ( $Fr_{\text{min\_SW}}$ ) is:

$$Fr_{\text{min\_SW}} = 6.057 \times (VJ)^{0.377} = 0.735$$

Comparing the results with the design standards from the PUB\_COP\_7th\_Edition[7] in Singapore, which suggests a design Froude number of 0.8, we find that  $Fr_{\text{min}}$  is very close to this standard. According to JIA's study[4],  $Fr_{\text{min}}$  represents the most stable condition of the channel. Therefore,  $Fr_{\text{min\_SW}}$  can be considered an appropriate stability indicator for the study area, representing the river channel's most stable state.

The optimization effects were analyzed by comparing  $Fr_{\text{min\_SW}}$ ,  $Fr_{\text{pre}}$  and  $Fr_{\text{O}}$  with respect to performance indicators. The following graph shows the variance analysis along the downstream flow direction.

Upon analyzing the boxplot, several key observations can be made:

- 1) The distribution of  $Fr_{\text{O}}$  is more concentrated, with 75% of the values below 1, indicating a more stable flow condition that avoids prolonged supercritical flow.
- 2) The distribution of  $Fr_{\text{pre}}$  is significantly more dispersed, with approximately 30% of the values exceeding 1, indicating highly unstable flow conditions.
- 3) The median of  $Fr_{\text{O}}$  shows a lower variance in the stability index compared to  $Fr_{\text{pre}}$ , although it remains close.

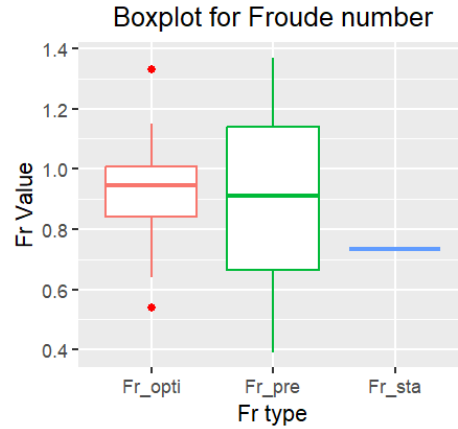


Fig. 9 Boxplot for Comparison of Fr

From this statistical analysis, it can be concluded that the optimized channel demonstrates improved stability compared to the natural channel.

### 3.2. Submerged Trapezoidal Weirs

This section examines submerged trapezoidal broad-crested weirs under varying upstream face slopes, focusing on long-term average water level flow conditions. The flow behavior observed is as follows: upstream of the weir, the flow is subcritical ( $Fr_1 < 1$ ); over the weir crest, a critical flow transition occurs; and downstream, the flow becomes supercritical ( $Fr_2 > 1$ ), eventually returning to subcritical flow further downstream.

The simulation results presented below illustrate these flow properties through graphs and charts.

#### 3.2.1. Flow Surface Profile

The computed free surface elevation is used to plot the streamlines over the three types of weirs under constant discharge conditions (See Fig. 10). The water surface profile at the downstream end of the weir depends on the initial water level and is not the primary focus of this analysis.

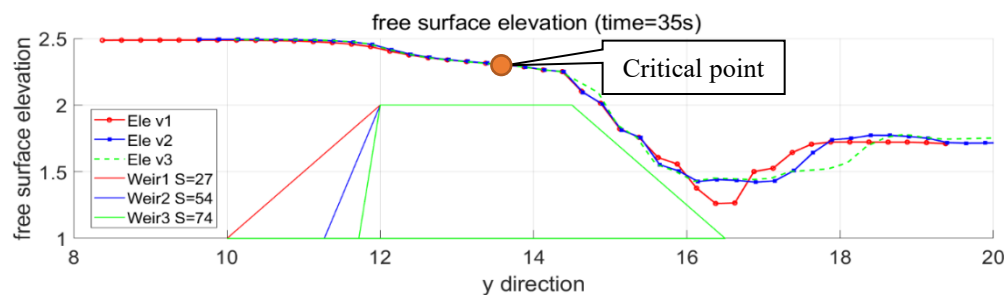


Fig. 10. computed water-surface profile over the weirs

In practice, undular flow can lead to pressure redistribution and potential damage to hydraulic structures, a condition that must be avoided in river engineering. Fig. 10 demonstrates that the current weir design avoids the formation of undular flow. This can be confirmed by applying the criterion for undular flow formation [8]:



$$\frac{H_0 - Z}{L_{cr}} < 0.15 \quad (3-1)$$

where numerator  $H_0 - Z$  represents the upstream head above the weir crest, and the weir crest length  $L_{cr}=2.5m$ . In this case:

$$\frac{H_0 - Z}{L_{cr}} = 0.2 < 0.5$$

indicating that the flow over the weir typically forms a parallel streamline. Notably, as the slope ( $\theta$ ) increases, the hydraulic jump downstream shifts further away from the weir heel.

### 3.2.2. Critical point

The weir effectively controls the discharge, causing the flow over the weir to transition into a supercritical state (See Fig. 11).

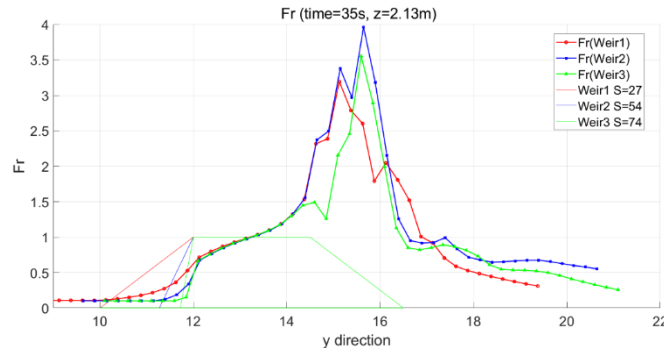


Fig. 11. Froude number along the stream

The first transition to critical flow occurs on the crest, and the upstream slope does not significantly alter the location of this transition. The Froude number reaches its peak near the weir heel. When combined with the water profile, it is evident that Weir 2, which has a higher  $Fr$ , exhibits faster velocity and lower water depth, potentially increasing the risk of erosion.

### 3.2.3. Velocity distribution

Fig. 13 illustrates the velocity distribution by 3D velocity magnitude, with the maximum vertical velocity values extracted in Table. 4.

The overall velocity distribution along the streamline can be described as follows:

- 1) Upstream of the weirs, the velocity profiles are straight and uniform.
- 2) Flow velocity gradually increases as the water reaches the weirs. Compared to mild upstream slopes, a steeper slope results in a sharp velocity increase at the corner of the weir. Steep slopes or shallow water depths cause the flow to slow significantly behind the weir, leading to water accumulation and reduced discharge over the weir. The discharge for submerged trapezoidal weirs in open channels can be calculated by:

$$Q = C_D B \sqrt{2gH}$$

where  $H$  is total overflow head, it can be illustrated that the steep slopes reduce the discharge coefficient  $C_D$ . [9]

- 3) Downstream of the weirs, the maximum vertical velocity typically occurs near the

weir heel. Although mild slopes result in relatively lower average velocity magnitudes, they produce significantly higher vertical velocities. Conversely, steep slopes lead to minimal vertical velocity and relatively lower average velocity magnitudes.

Table. 4 Maximum vertical velocity along downstream face of weir

| Weir | Max w (m/s) | Distance to heel(m) |
|------|-------------|---------------------|
| 1    | 2.12        | 0.625               |
| 2    | 1.91        | 1.855               |
| 3    | 1.40        | 1.655               |

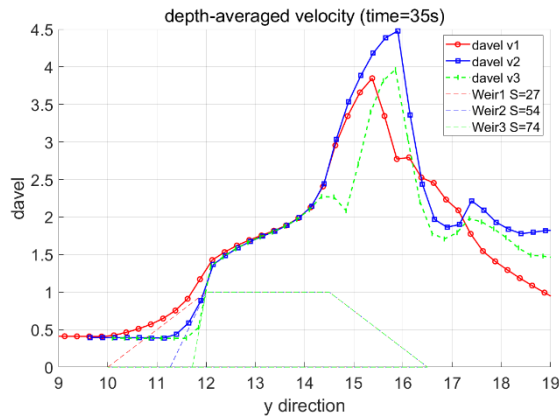


Fig. 12. Depth-averaged velocity (unit: m/s)

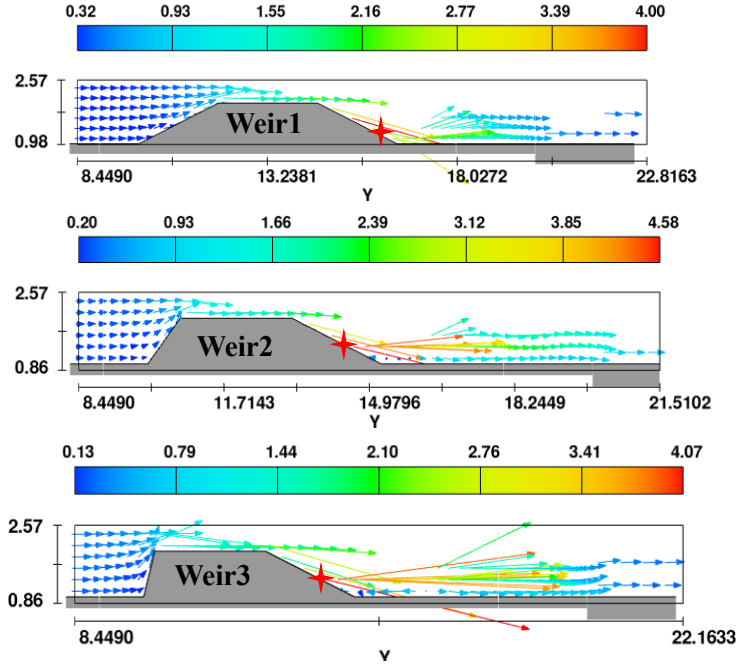


Fig. 13 Velocity distribution

- 4) Compare the flow velocity profile before and after weir in Fig. 14, where the downstream measurement distance is 2m from the heel. In the velocity profile after the Weir 3, a sudden change was observed.

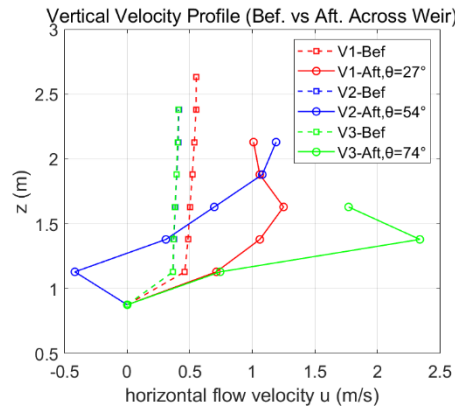


Fig. 14 Comparison of flow velocity profile before and after weir

### 3.2.4. Turbulence Over Weirs

Turbulence typically occurs before and after weirs, causing energy losses, noise, and structural vibrations. The optimal design of weirs aims to minimize these effects. To evaluate the turbulence downstream of the weirs, the turbulence intensity  $I$  is calculated as follows:

$$I = \sqrt{\frac{k_T}{K}} \quad (3-2)$$

where  $k_T$  is the turbulent kinetic energy,  $\bar{K}$  is the mass-averaged mean kinetic energy in the domain. [6]

The results show that similar turbulence intensities occur downstream of all weirs (See Fig. 15), though Weir 3 (with a steep slope) produces a smaller turbulence range. This suggests that steeper slopes reduce turbulence and its associated negative effects.

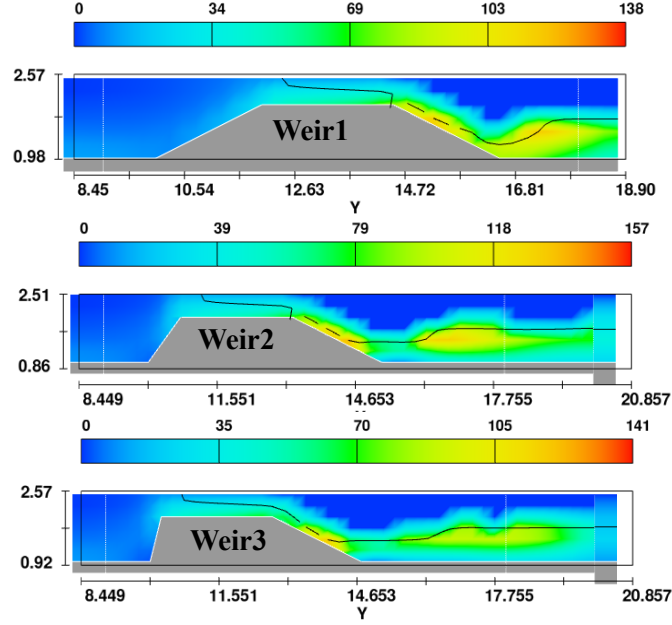


Fig. 15. Turbulence Intensity (unit: %)

### 3.2.5. Sediment Transport

Sediment transport is generally composed of two components: suspended load and bedload. In the Shawan Channel, the primary sediment is sand with  $d=0.2mm$ .

#### 1) Bed-Load Sediment

To quantify bedload transport, a common approach[10] is to use the non-dimensional Einstein number  $q_b^*$  for well-sorted sediments. One of the popular bedload transport relations from Engelund and Fredsoe's work [11]:

$$q_b^* = 18.74(\tau^* - \tau_c^*)(\tau^{*0.5} - 0.7\tau_c^{*0.5}), \quad \tau_c^* = 0.05 \quad (3-3)$$

Where  $\tau^*$  is the Shields stress, calculated as:

$$\tau^* = \frac{\tau_b}{\rho R g D} \quad (3-4)$$

And  $\tau_b$  is the bed shear stress, which can be expressed using the Chezy coefficient  $C$ :

$$\tau_b = \frac{\rho g}{C^2} V^2 \quad (3-5)$$

where  $V$  is the magnitude of flow velocity.

Given the lower vertical velocity and average velocity magnitude in Weir 3, the steeper upstream slope helps reduce sediment transport and possibly mitigates erosion to some extent.

#### 2) Simplified Analysis without Water Depth Consideration

The Hjulström-Sundborg diagram (Fig. 16) is a useful tool for understanding the erosion, transport, or deposition of sediment grains. However, it does not account for water depth.

Given that the sand in the Shawan River has a diameter of approximately  $D=0.2 mm$

and the velocity downstream of the weir exceeds  $1 \text{ m/s}$ , erosion is highly probable. It's essential to recognize that while sedimentation results from velocity deceleration, erosion occurs due to velocity acceleration, which the Hjulström curves do not consider.

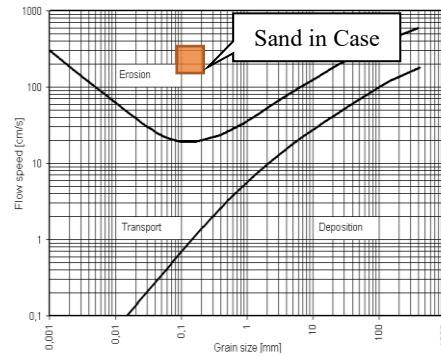


Fig. 16. Hjulström-Sundborg diagram

### 3) Suspension Sediment in SRD

The suspension concentration and conditions near the bedform can be analyzed using the effective Shields parameter  $\theta'$  and the particle Reynolds number  $R_p$  within the context of the Shields Regime Diagram (SRD). For fine sediment particles, the critical parameters can be explicitly defined[12] using the particle Reynolds number  $R_p$ , calculated as:

$$R_p = \frac{Re}{\sqrt{\theta}} = \frac{\sqrt{(s-1)gd}d}{\nu} \quad (3-6)$$

where  $R_p$  depends (among other things) on the sediment size  $d$ , but not other hydrodynamic factors.

Then, the dimensionless Shields parameter  $\theta$  is expressed as:

$$\theta = \frac{uf^2}{(s-1)gd} \quad (3-7)$$

where  $s$  is the specific gravity of sediment. The effective Shields parameter  $\theta'$  distinguishes between different bedform regimes:

- For the upper regime ( $\theta' > 0.55$ ):  $\theta' = [0.702\theta^{-1.8} + 0.298]^{-1/1.8}$ ;
- For the lower regime ( $\theta' \leq 0.55$ ):  $\theta' = 0.3\theta^{1.5} + 0.06$ .

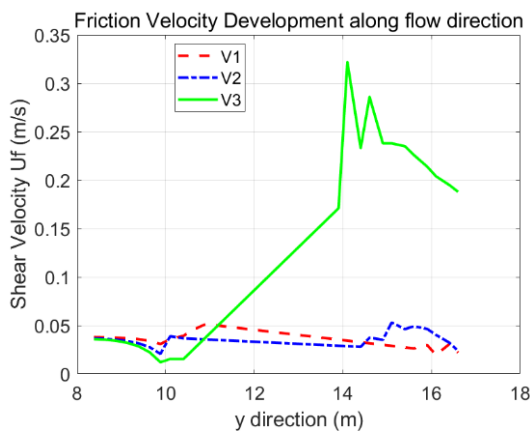


Fig. 17 Shear Stress

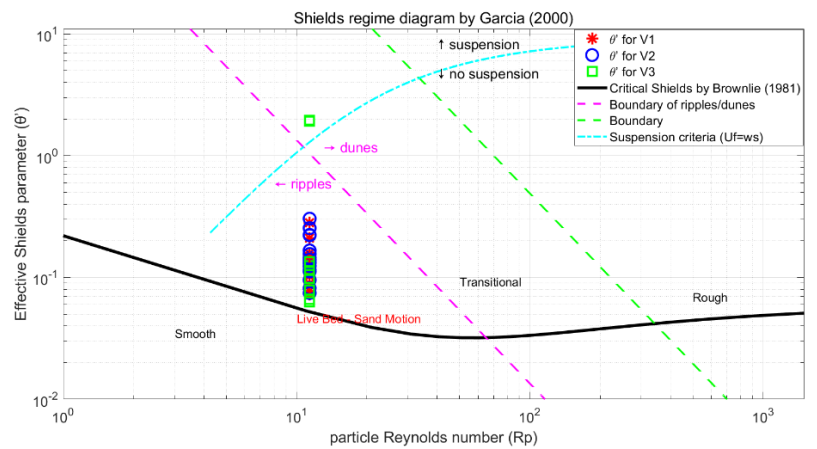


Fig. 18 SRD

Based on the analysis using the SRD (See Fig. 17~18), the steep upstream slope in Weir

3 results in significant velocity changes and locally elevated shear stress, which promotes greater sediment suspension and reduces the likelihood of sedimentation.

## 4. Conclusion

### 4.1. Optimization channel

- 1) Under conditions of long-term average discharge and water levels, the optimized channel exhibits a lower peak value relative error ( $\sigma$ ) and demonstrates greater stability compared to the natural channel.
- 2) During a 100-year return period storm event, the correlation coefficient for the optimized channel exceeds 0.8, indicating stronger performance in extreme conditions. Overall, the optimized channel outperforms the natural channel in handling such extreme scenarios.

### 4.2. Suitable Shape of Trapezoidal-Board Weir

Based on the comparison of different weir designs in terms of flow dynamics and sedimentation in Table. 5, the following conclusions can be drawn:

- 1) The design of the weir crest successfully prevents the formation of undular flow.
- 2) Flow over the weir generally follows a parallel streamline, ensuring a smooth transition.
- 3) To accommodate a higher flow capacity, a mild upstream slope is preferable, as it enhances flow efficiency.
- 4) A steeper upstream slope increases shear stress near the downstream heel, significantly raising the potential for erosion in that area.
- 5) From a stability perspective, a steeper upstream slope positively influences overall flow stability.

Table. 5 Analysis of Hydraulic Performance for Various Weir Slopes

| Weir   | Flow Condition  | Velocity distribution  | Turbulence                   | Sediment transport  |
|--|---|--|------------------------------|---|
| No. 1<br>$\theta=27^\circ$<br>Mild Slope     | 1) No undular flow;<br>2) Parallel streamline.  | 1) Relatively lower averaged velocity magnitude;<br>2) High vertical velocity may damage hydraulic structures. | Largest range of turbulence. | Stable sheart stress, reduces suspension sediment transport.        |
| No. 2<br>$\theta=54^\circ$<br>Moderate Slope | Too high $Fr$ values  | -  | -                            |   |
| No. 3<br>$\theta=74^\circ$<br>Steep Slope    | 1) Smoother and flatter water profile;<br>2) Hydraulic jump shifts far downstream from the weir heel. | 1) Reduces discharge coefficient $C_D$ ;<br>2) Minimum vertical velocity and low average velocity magnitude.   | Smallest range of turbulence | Higher shear stress increases the likelihood of downstream erosion. |

## References

- [1] S. E. Greco and E. W. Larsen, 'Ecological design of multifunctional open channels for flood control and conservation planning', *Landscape and Urban Planning*, vol. 131, pp. 14–26, Nov. 2014, doi: 10.1016/j.landurbplan.2014.07.002.
- [2] Shenzhen Water Bureau, 'Preliminary Design Report on River Training in Shawan River Basin of Shenzhen', Sep, 2015.
- [3] DHI MIKE User Manual.
- [4] Y. Jia, 'Minimum froude number and the equilibrium of alluvial sand rivers', *Earth Surf. Process. Landforms*, vol. 15, no. 3, pp. 199–209, May 1990, doi: 10.1002/esp.3290150303.
- [5] M. R. Madadi, A. Hosseinzadeh Dalir, and D. Farsadizadeh, 'Investigation of flow characteristics above trapezoidal broad-crested weirs', *Flow Measurement and Instrumentation*, vol. 38, pp. 139–148, Aug. 2014, doi: 10.1016/j.flowmeasinst.2014.05.014.
- [6] FLOW-3D, 2012. FLOW-3D User Manual. Flow Science Inc.
- [7] 'PUB\_COP\_7th\_Edition in Singapore.pdf'. Accessed: Oct. 09, 2023. [Online]. Available: [https://www.pub.gov.sg/Documents/PUB\\_COP\\_7th\\_Edition.pdf](https://www.pub.gov.sg/Documents/PUB_COP_7th_Edition.pdf)
- [8] O. Castro-Orgaz and H. Chanson, 'Near-critical free-surface flows: real fluid flow analysis', *Environ Fluid Mech*, vol. 11, no. 5, pp. 499–516, Oct. 2011, doi: 10.1007/s10652-010-9192-x.
- [9] H. M. Fritz and W. H. Hager, 'Hydraulics of Embankment Weirs', *Journal of Hydraulic Engineering*, vol. 124, no. 9, pp. 963–971, Sep. 1998, doi: 10.1061/(ASCE)0733-9429(1998)124:9(963).
- [10] M. H. Chaudhry, *Open-Channel Flow*. Cham: Springer International Publishing, 2022. doi: 10.1007/978-3-030-96447-4.
- [11] J. Fredsoe and R. Deigaard, *Mechanics of Coastal Sediment Transport*, vol. Volume 3. in Advanced Series on Ocean Engineering, no. Volume 3, vol. Volume 3. WORLD SCIENTIFIC, 1992. doi: 10.1142/1546.
- [12] R. A. Gaines and R. H. Smith, 'Micro-Scale Loose-Bed Physical Models', in *Hydraulic Measurements and Experimental Methods 2002*, Estes Park, Colorado, United States: American Society of Civil Engineers, Oct. 2002, pp. 1–12. doi: 10.1061/40655(2002)78.